



On the radicalar properties of graphene fragments: double-hybrid DFT and perturbation theory approaches

Michele A. Salvador¹ · Felipe C. T. Antonio¹ · Gabriela D. da Silva¹ · Fernando H. Bartoloni¹ · Ednilsom Orestes² · Mauricio D. Coutinho-Neto¹ · Paula Homem-de-Mello¹

Received: 10 March 2020 / Accepted: 8 June 2020 / Published online: 19 June 2020
© Springer-Verlag GmbH Germany, part of Springer Nature 2020

Abstract

The physical–chemical properties of polycyclic aromatic hydrocarbons (PAHs), molecules formed by fused carbon rings passivated by hydrogen atoms, make them attractive to several applications, including light-emitting diodes, photovoltaic cells, and transistors. They borrow some of the unique properties of graphene, nanotubes, and fullerenes. Additionally, radicals related to these structures may be involved in carcinogenic effects. In this work, electronic and energetic aspects of PAHs, including triangulenes, were analyzed using BLYP and B2PLYP density functionals as well as with unrestricted Hartree–Fock (UHF) and second-order Møller–Plesset perturbation (MP2) theories. The results show that DFT BLYP and B2PLYP functionals predict adiabatic singlet–triplet energy gap in better agreement to reference data when compared to MP2, with the double-hybrid B2PLYP producing better results than BLYP. On the other hand, for calculation of properties involving radical species, as homolytic bond dissociation energies, B2PLYP overestimates the binding energy, especially for larger PAHs. The erratic behavior of UHF and MP2 for open-shell species limits the B2PLYP performance regarding the stability analysis of triangulenes over different multiplicities.

Keywords Polycyclic aromatic hydrocarbons · Density functional theory · Møller–Plesset perturbation theory · Bond dissociation energy · Triangulenes · Multiplicity

1 Introduction

Polycyclic aromatic hydrocarbons (PAHs) are a class of very stable aromatic organic molecules, formed by fused benzenoid rings passivated by hydrogen atoms [1]. They are supposed to be prevalent in the interstellar medium, representing between 10 and 20% of the total interstellar carbon [2, 3], and have been proposed as the carriers of aromatic infrared bands (AIBs). They are also very abundant in our local environment since they are a result of natural processes as biomass burning and by-products of fossil fuels incomplete combustion [4], which have become a problem since they are suggested to be carcinogens, mutagens, and teratogens [5]. Genotoxicity of PAHs largely depends on initial supra-molecular interactions with the DNA, regulated by electron charge distribution and geometric distortions [6]. The latter is particularly relevant to determine the PAH affinity toward individual nucleotide bases, for example, with planar and non-planar derivatives binding with higher affinities guanine and adenine nucleotides, respectively [6]. It is also known that increased non-planarity lowers the capability of

“Festschrift in honor of Prof. Fernando R. Ornellas” Guest Edited by Adélia Justino Aguiar Aquino, Antonio Gustavo Sampaio de Oliveira Filho and Francisco Bolivar Correto Machado.

Electronic supplementary material The online version of this article (<https://doi.org/10.1007/s00214-020-02632-w>) contains supplementary material, which is available to authorized users.

✉ Michele A. Salvador
michelesalvador@gmail.com

✉ Paula Homem-de-Mello
paula.mello@ufabc.edu.br

¹ Centro de Ciências Naturais e Humanas, Universidade Federal do ABC, Av. dos Estados, 5001, Santo André, SP 09210-580, Brazil

² Escola de Engenharia Industrial Metalúrgica, Universidade Federal Fluminense, Av. dos Trabalhadores, 420, Volta Redonda, RJ 27255-125, Brazil

the PAH to be metabolized and ultimately produce DNA-damaging adducts [7, 8]. Biological damage provoked by PAHs involves the formation of covalent bonds following supramolecular interactions, with the hydrocarbons acting as electrophiles while DNA and proteins act as the nucleophilic species. PAHs reactivity is often connected to the generation of intermediate stable radical compounds [6, 9].

The dependency of PAHs properties on their size and structure makes them amenable for applications as light-emitting diodes, photovoltaic cells, and transistors [10]. They have many of the properties presented by their larger allotropic relatives, such as graphene, nanotubes, and fullerenes [11, 12], and can be considered as their constituent elements. The interaction of small molecules with PAHs has been extensively investigated using theoretical methods. Donchev [13] studied the molecular hydrogen interaction with PAHs up to coronene ($C_{24}H_{12}$) using second-order Møller–Plesset (MP2) perturbation theory. It was found that the electrostatic energy component played an essential role in PAH– H_2 interactions, and the energetic preference for the perpendicular H_2 orientation over the parallel one decreases rapidly as PAHs size increases. Zhechkov et al. [14] studied the physisorption of N_2 on PAHs C_6H_6 , $C_{10}H_8$, $C_{14}H_{10}$, $C_{22}H_{14}$, $C_{18}H_{12}$ and $C_{24}H_{12}$ at MP2 level of theory, aiming to identify the relations among PAHs interaction energies, size, and structures. They have found that binding energies increase with the PAH polarizability, which is correlated with PAH size. Density functional theory (DFT) has been shown to be a valuable tool to study those interactions. Tachikawa et al. [12] investigated the adsorption of atomic hydrogen on graphene nanoflakes (PAHs: $C_{42}H_{16}$, $C_{54}H_{18}$, $C_{78}H_{22}$ and $C_{96}H_{24}$) using CAM-B3LYP functional; Wagle [15] obtained the binding energies, orbital energies, and charge transfer behavior considering the sorption of 12 different ionic liquids (ILs) onto six different PAHs with B3LYP functional; and Chakarova-Käck [16] proposed a functional, called vdW-DF, to study the stacking of PAHs (benzene, naphthalene, anthracene, and pyrene), and estimated the exfoliation energy of graphene sheets.

Excited states and open-shell forms of PAHs have been investigated in an accurate scheme, by means of first principles coupled-cluster calculations [17–20]. However, the computational cost of the calculations described on the previous paragraphs may become an issue, and MP2 and DFT approaches could be less expensive alternative methodologies. Parac and Grimme [21, 22] evaluated time-dependent density functional theory (TDDFT)-based approaches to obtain vertical excitation energies for PAHs, but B3LYP and the pure gradient-corrected BP86 presented considerable errors [21]. Buragohain et al. [23] studied the electronic transitions of pyrene ($C_{16}H_{10}$), perylene ($C_{20}H_{12}$), coronene ($C_{24}H_{12}$), and heptacene ($C_{30}H_{18}$) in neutral (PAH), protonated (HPAH⁺) and deuterated (DPAH⁺) forms, by means

of TDDFT-BLYP calculations. Protonated and deuterated isomeric forms of PAHs showed more electronic transitions in the visible wavelength range than the corresponding neutral PAH that increased with molecular weight.

Powell et al. studied the fluorescent spectra of three $C_{24}H_{14}$ isomers and a PAH containing heteroatoms. Best predictions were achieved by using CAM-B3LYP functional, and by including the influence of the solvent [24]. Yadav et al. [25] studied the similarities and differences between electron density, spin density, and MEP pattern distributions in ground and lowest π – π^* excited states of $C_{26}H_{16}$, $C_{28}H_{14}$, $C_{38}H_{22}$ and $C_{68}H_{22}$, aiming to obtain their photochemical reactivity. They also evaluated possible application of PAHs in solar energy-harnessing technology, by analyzing the oscillator strengths of electronic absorption transitions.

Allison et al. [5] determined with B3LYP and MP2-based methodologies the enthalpies of formation for 669 PAH compounds and a set of functionalized molecules. To do so, they have used an empirical method to predict the thermochemical properties of compounds as sums of the properties of their components, called ‘group additivity.’ The largest PAH considered in this study had a molecular formula of $C_{38}H_{22}$. Their methodology has proved reliable to predict the thermochemical properties with good accuracy.

An important feature of PAHs is the stability of generated radicals after homolytic hydrogen abstraction. Due to the genotoxicity of radical species, some studies have been conducted to predict the bond dissociation energy of PAHs (see, for example, Refs. [26, 27]). However, there is a limited amount of studies relating polyradicaloid PAH molecules, which contain unpaired electrons due to topological effects [17, 18, 28]. Such systems are known to exhibit an increasing polyradical character with the number of fused benzene rings. Pérez-Guardiola et al. [29] studied these systems as representing the shortest segment of armchair or zigzag single-walled carbon nanotubes, using finite-temperature (FT)-DFT. It has shown the intricate and delicate interplay between structural and electronic effects in carbon-based structures, particularly challenging in the case of polyradicaloid molecules.

Phenalenyl ($C_{13}H_{10}$) is a PAH which presents a high-spin open-shell radical character in its ground state [30, 31]. The addition of benzene rings in this structure keeping its triangular form can lead to several π -conjugated phenalenyl derivatives, such as triangulene, also known as Clar’s hydrocarbon [32]. It exists as a diradical containing an even number of carbons, because it has two unpaired electrons, and it is considered as the smallest triplet-ground-state polybenzoid [32, 33].

Sharma et al. [33] investigated triplet (ferromagnetic) and singlet (antiferromagnetic) states for triangulene. Their main goals were to study its electronic and vibrational properties in the ground state, to analyze the effects of transition metals

on electronic and magnetic properties, and also to determine global reactivity descriptors as polarizability, global hardness, electrophilicity, and additional electronic charge. It was found that the ferromagnetic (triplet) state was more stable, which was confirmed by vibrational frequencies and by global reactivity descriptor analyses.

Ciolowsky et al. [26] obtained bond dissociation energies (BDE) for some PAHs at the BLYP level of theory, as well as May et al. [34] at B3LYP and BP86 levels, and Barckholtz et al. [27] at UHF, MP2, BLYP and B3LYP, among others. DFT has accurately predicted BDEs for C–H bonds of benzene and small PAHs with an even number of carbon atoms.

The aim of this work is to assess the performance of distinct popular electronic structure methods, based on DFT and MP2 approaches, to compute multiplet energy differences and BDEs for different classes of PAHs. In this work, we have extended the Ciolowsky et al. [26] investigation on PAHs to structures with more than 18 carbon atoms, structures with even an odd number of carbon atoms and triangulenes, and the performance of the distinct methods was measured against both experimental and reference theoretical data available in the literature.

2 Methods

The ab initio second-order Møller–Plesset perturbation theory (MP2) [35–37], and density functional theory (DFT) [38–40] approaches, as implemented in the ORCA 3.0.3 package [41, 42], have been applied to investigate the structure, energetics, and electronic states of all 24 PAHs studied in this work. The geometries of all PAHs were fully optimized using the BLYP [43, 44] functional with inclusion of the D3 dispersion correction method [45]. The geometry optimizations were followed by vibrational frequency calculations in the same level of theory to ensure that all structures correspond to a true minimum on the potential energy surface.

The 6-311G(*d*) basis set was used for geometry optimization and for the subsequent single-point calculations of all PAHs. As the functional and the basis set chosen for the geometry optimization is the same for all PAHs analyzed in this work, thus, such information will be omitted

henceforth. The basis set selection was based on previous works already described here, which use, in most cases, Ahlrichs def2 [17, 20, 29, 46] and split-valence Pople [1, 12, 33, 47] basis set families in most cases, with Dunning cc-pVnZ family [5, 24] being less common. Sure et al. [48] presented an extensive review of basis set—functional combinations, critically discussing the more appropriate sets for the evaluation of different properties evaluations of PAHs, including the sources of errors and the role of long-range interactions. Barckholtz et al. [27] performed a basis set benchmark study on BDE values of PAHs comparing single-point calculations based on Pople basis sets 6-31G(*d*), 6-311 + G(*d,p*) and 6-311 + G(3*df*,2*p*) along with B3LYP functional and authors pointed out no significant differences in either smaller or larger basis, with higher angular momentum and diffuse functions. A systematical comparison of benzene BDE values evaluated with different levels of theory (HF, DFT and MP2) and basis sets (SV(P), SVP, TZVP, and TZVPP), performed by May et al. [34], shows that for HF and DFT levels of theory, both with different basis set, similar results were obtained; for MP2, more substantial variations were observed. Moreover, DFT results with the mentioned basis sets were compared with UHF/6-31G and B3LYP/6-311G(*d,p*) found in the literature, reaching a good agreement with both. Based on these findings and on the complexity of variables we are interested in, we have chosen Pople basis 6-311G(*d*) for the calculations reported in this work.

The lowest singlet and triplet excited states, used to calculate the corresponding adiabatic energy differences (AE_{ST}) of the selected PAHs shown in Table 1 (and Table SM2), were obtained with single-point energy calculations using MP2, the BLYP functional with D3 dispersion correction, and the B2PLYP functional with D3 with Becke–Johnson damping (D3BJ) [49]. These AE_{ST} results were compared with reference CCSD(T) single-point energy calculation over B3LYP geometries using the cc-pVTZ basis set [50]. The carbon-hydrogen homolytic bond fission that gave the most stable radical isomer for each PAH shown in Table 2 was evaluated using BLYP and B2PLYP single-point energy calculations over BLYP optimized geometries. The total energy of the triangulenes, shown in Table 3, which can be experimentally generated from specific bond-breaking patterns from graphene sheets, were calculated after proper

Table 1 Adiabatic singlet–triplet energy gaps (AE_{ST} , in eV) and errors, in parenthesis, regarding CCSD(T) calculations [50]

Compound ^a	CCSD(T)// B3LYP [50]	BLYP//BLYP	B2PLYP//BLYP	MP2//BLYP	UHF//BLYP
Perylene (C ₂₀ H ₁₂)	1.71	1.35 (− 0.21)	1.83 (0.07)	3.73 (1.18)	0.46 (− 0.73)
Pyrene (C ₁₆ H ₁₀)	2.22	1.94 (− 0.13)	2.34 (0.05)	3.20 (0.44)	1.26 (− 0.43)
Chrysene (C ₁₈ H ₁₂)	2.79	2.27 (− 0.19)	2.69 (− 0.04)	5.55 (0.99)	1.36 (− 0.51)
Phenanthrene (C ₁₄ H ₁₀₋₂)	2.92	2.56 (− 0.12)	3.07 (0.05)	5.26 (0.80)	1.42 (− 0.51)

^aChemical formula and, for phenanthrene, isomer identification, as in Table 2

Table 2 Bond dissociation energies (BDE, in kcal mol⁻¹) obtained for the extraction of different hydrogen atoms in PAHs with an even number of carbon atoms, calculated with BLYP and B2PLYP on BLYP geometries

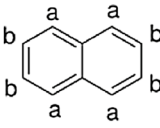
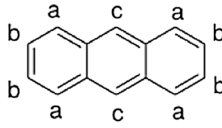
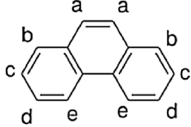
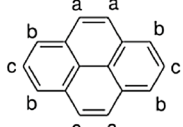
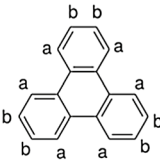
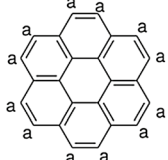
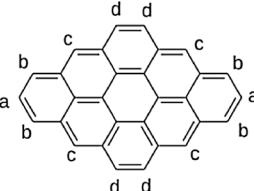
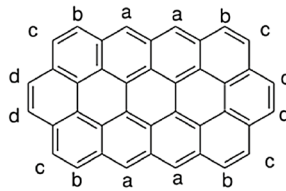
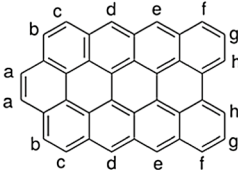
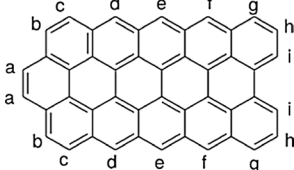
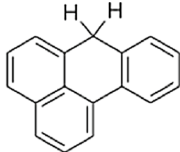
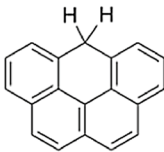
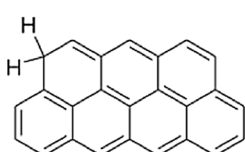

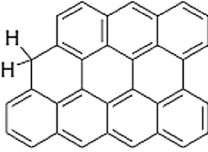
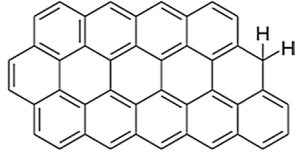
Abstracted H	BLYP	B2PLYP	BLYP	B2PLYP
				
	$C_{10}H_8$		$C_{14}H_{10}$	
a	115.1	116.3	115.1	118.9
b	115.1	115.9	115.1	116.6
c	–	–	115.3	116.2
				
	$C_{14}H_{10_2}$		$C_{16}H_{10}$	
a	115.0	116.1	114.6	115.3
b	115.1	116.0	115.1	117.1
c	115.2	116.2	114.6	115.1
d	115.0	115.8	–	–
e	113.4	114.3	–	–
				
	$C_{18}H_{12}$		$C_{24}H_{12}$	
a	112.7	113.5	115.2	113.2
b	115.1	116.0	–	–
				
	$C_{30}H_{14}$		$C_{40}H_{16}$	
a	116.4	131.9	117.8	136.3
b	117.2	133.4	117.3	116.0
c	117.2	133.1	117.2	135.6
d	116.6	131.9	117.4	116.0
				
	$C_{38}H_{16}$		$C_{46}H_{18}$	

Table 2 (continued)

a	117.3	158.3	115.2	158.2
b	117.1	160.5	115.0	137.9
c	117.2	134.6	120.1	136.2
d	117.7	136.5	115.4	138.1
e	117.7	149.1	115.2	145.7
f	117.7	136.1	115.2	148.1
g	116.9	136.1	115.4	157.5
h	115.7	133.9	119.4	137.3
i	–	–	113.4	135.9

Table 3 Bond dissociation energies (BDE, in kcal mol⁻¹) obtained with BLYP and B2PLYP, both on BLYP geometries, for the extraction of the hydrogen atom bonded to the *sp*³ carbon in PAHs with an odd number of carbon atoms

 $C_{17}H_{12}$ BLYP = 68.4 B2PLYP = 75.9	 $C_{19}H_{12}$ BLYP = 67.4 B2PLYP = 75.9	 $C_{25}H_{14}$ BLYP = 42.6 B2PLYP = 48.3
 $C_{27}H_{14}$ BLYP = 65.6 B2PLYP = 76.1	 $C_{33}H_{16_2}$ BLYP = 52.4 B2PLYP = 66.5	 $C_{43}H_{18}$ BLYP = 54.1 B2PLYP = 74.4

hydrogen atoms passivation. These results were evaluated using BLYP optimized geometries and MP2, BLYP, B3LYP [44, 51–53], and B2PLYP single-point energy calculations at different multiplicities due to their radical character. An additional B2PLYP single-point energy calculation over D3BJ-B2PLYP optimized geometries was also included for comparison (Table SM3). BLYP, B3LYP, B2PLYP functionals, as well as MP2 and UHF methods, were used to compare the relative energies among multiplets of the naturally occurring ground-state radical forms of the triangulenes studied in this work.

3 Results and discussion

3.1 Singlet–triplet energy gap and bond dissociation energy

The performance of the selected methods for singlet–triplet energy gaps was assessed for the compounds shown in Table 1 (and Table SM2). Our results were compared to

CCSD(T) reference calculations which in turn are in good agreement with experimental values [50]. As it can be seen, the singlet–triplet energy gap is quite well reproduced by B2PLYP (using BLYP optimized geometries) and show considerable improvement over the results obtained using BLYP. On the other hand, the MP2 singlet–triplet energy gaps are overestimated compared to reference data. Unrestricted Hartree–Fock (UHF) calculations were included to shed light into the behavior of MP2 and (to a less extent) B2PLYP calculations. The results from UHF single-point energy calculations underestimate the energy gap by a comparable amount and display strong spin contamination (this will be further discussed below—see Figs. 1, 2); this results in overstabilization of the radical species as indicated by BDE estimates [26].

In this case, due to the fact that the UHF zeroth-order reference is contaminated, MP2 may also present difficulties in singlet–triplet gap and BDE calculations, as seen before [54]. Moreover, previous calculations for PAHs and nanographenes, in which relativistic spin-coupling phenomena were taken into account, as well as sophisticated methods

Site	BLYP	B3LYP	B2PLYP	UHF
b				
S^2	0.7866	1.0340	1.2751	5.2657
g				
S^2	0.7672	0.8075	2.2867	6.1911

Fig. 1 Spin density calculated with different methods for two $C_{38}H_{15}$ radical species ('sites' refer to hydrogen abstraction indicated in Figure SM1). Isosurfaces value = 0.07 e/au^3 . The green surface refers to

an excess density of alpha spin, while the red surface to an excess density of beta spin. S^2 refers to expectation value of the total spin-squared operator

for singlet–triplet gaps and spin–orbit coupling, showed that DFT approaches are adequate to obtain ground-state properties, especially when intrinsic magnetism is negligible. Magnetism may occur in nanographene structures when defects are present [18, 55] or for singlet open-shell biradicaloids, namely zethrenes, for which Das and co-workers [17] have shown that high-level theoretical multireference methods are more appropriate tools to describe their electronic structure.

We have calculated the bond dissociation energies (BDE) between hydrogen and carbon atoms for a series of compounds shown on Tables 2 and 3. Structures with even number of carbon atoms have only sp^2 hybridized carbons, while structures with odd number of carbon atoms can present different isomers (see Table SM1, for total electronic energies) depending on the position of the sp^3 carbon (except for triangulenes, presented in next section). BDE results for the most stable isomer of each PAH are shown in Tables 2 and 3.

Ciolowsky et al. [26] observed for PAHs with an even number of carbon atoms that the hydrogen atoms from “congested regions” are removed preferentially. In our calculations, these regions can be found in $C_{14}H_{10-2}$, sites *e*, in $C_{18}H_{12}$, sites *a*, $C_{38}H_{16}$, sites *h*, or sites *i* for $C_{46}H_{18}$. In these cases, BLYP and B2PLYP share the same trend with absolute BDE values in quite good agreement with previous works [26, 34, 56].

However, for larger PAHs ($C_{38}H_{16}$, $C_{40}H_{16}$ and $C_{46}H_{18}$), the differences in BDE for different hydrogen sites are predicted to be much larger when computed by B2PLYP than when BLYP is used. As reference, for large ‘even-PAHs’ that

present armchair and zigzag borders, in analogy to graphene sheets, May et al. [34] found that BDE at zigzag or armchair positions are similar differing by only 0.7 kcal mol⁻¹ in energy.

To further examine our findings, we compared spin densities computed using BLYP, B3LYP, B2PLYP functionals, and UHF for two possible radical species obtained from $C_{38}H_{16}$. The selected H-extraction sites were named *b* and *g*. These are quite similar sites, and the BDE difference is only 0.2 kcal mol⁻¹ as calculated by BLYP. However, this difference is estimated to be 24.4 kcal mol⁻¹ by B2PLYP calculations. We found that spin contamination increases as BLYP < B3LYP < B2PLYP < UHF resulting in very different spin density plots as shown in Fig. 1. As it can be seen from the presented surfaces, the more contaminated the wave-function, the more delocalized are the spin densities. B2PLYP spin density, for instance, is fairly delocalized and shows no spin density on carbon that has lost the hydrogen atom for site *b* (the dangling bond). This leads to poor accuracy on BDE values that get worse with increasing system size. The problem is analogous to the one observed for MP2 results on singlet/triplet stabilities (Table 1), where spin contamination on the UHF reference leads to poor MP2 energies.

For PAHs with an odd number of carbon atoms (Table 3), the BDE values calculated with BLYP functional decrease as the structures get larger, as expected, since the larger the conjugation system, the more stable the radical is. This is less evident for B2PLYP results. Figure 2 presents the

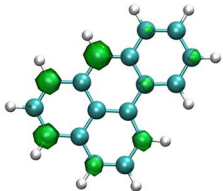
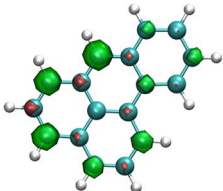
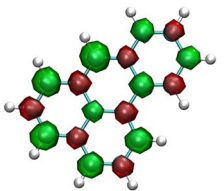
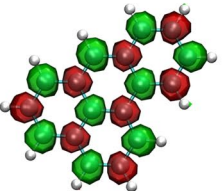
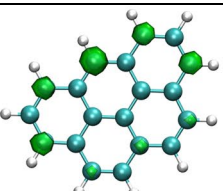
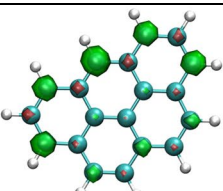
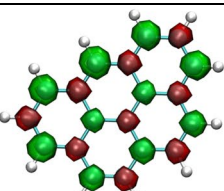
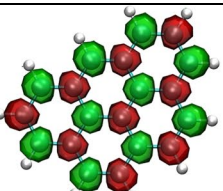
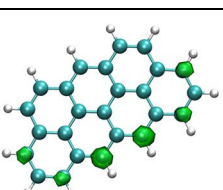
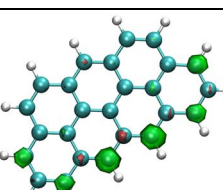
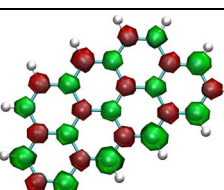
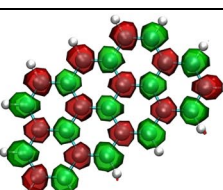
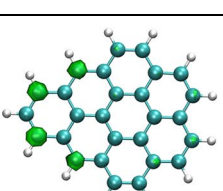
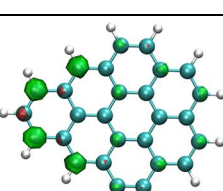
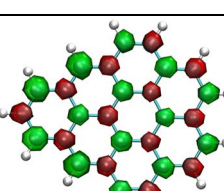
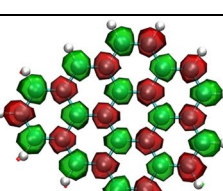
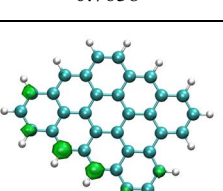
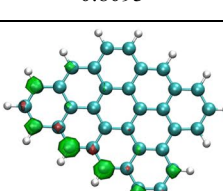
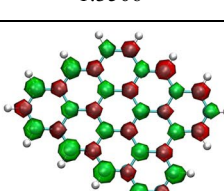
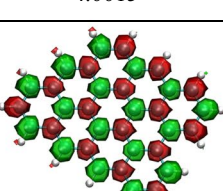
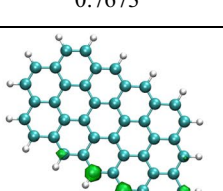
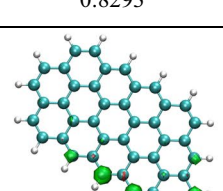
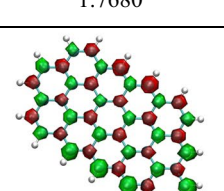
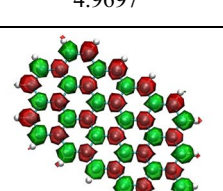
	BLYP	B3LYP	B2PLYP	UHF
$C_{17}H_{11}$				
S^2	0.7644	0.8016	1.0974	2.6314
$C_{19}H_{11}$				
S^2	0.7643	0.8048	1.1508	2.9047
$C_{25}H_{13}$				
S^2	0.7653	0.8119	1.3643	3.7945
$C_{27}H_{13}$				
S^2	0.7638	0.8093	1.3506	4.0015
$C_{33}H_{15_2}$				
S^2	0.7673	0.8293	1.7680	4.9697
$C_{43}H_{17}$				
S^2	0.7682	0.8447	2.1337	6.3645

Fig. 2 Spin density calculated with BLYP, B3LYP, B2PLYP, and UHF for radical species of PAHs with an odd number of carbons. Iso-surfaces value = 0.07 $e/a.u.^3$. The green surface refers to an excess den-

sity of alpha spin, while the red surface to an excess density of beta spin. S^2 refers to expectation value of the total spin-squared operator

spin densities obtained for ‘odd-PAHs.’ It is expected for radical species that the spin density spreads over the conjugated system with a pattern related to the node structure of the molecular orbital with the excess electron, since these structures have only sp^2 carbons. We observe that BLYP and B3LYP spin densities are localized at border carbon atoms, while B2PLYP and UHF ones are delocalized over the entire system. The observed spin localization at PAH edges is similar to the localization on zigzag-shaped edges of graphene nanoribbons [57]. As previously mentioned, the behavior on the results observed for B2PLYP and UHF seem to be a consequence of strong spin contamination in the single determinant wave-function.

3.2 Polyradicaloids: triangulene derivatives

Triangulenes (Fig. 3) are singular PAH species that are intrinsic radicals in their ground state [33, 58, 59]. Here, we evaluated triangulene energy differences for different multiplets (Fig. 4; Table SM3). The calculated ground state of the $C_{22}H_{12}$ and $C_{46}H_{18}$ PAHs were found to be of triplet and quintet multiplicity, respectively. For $C_{22}H_{12}$, the triplet state was predicted to be more stable than the singlet closed-shell one by 0.35 eV [59], and for $C_{46}H_{18}$, the quintet state was found to be lower in energy by 0.13 eV and 0.38 eV [58] than the triplet and singlet closed-shell states, respectively.

The results obtained with BLYP functional remarkably predicts a stable polyradical character (multiplicity = triplet for $C_{22}H_{12}$, quartet for $C_{33}H_{15}$, and quintet for $C_{46}H_{18}$) for all the compounds, in reasonable agreement with experimental and theoretical references. For $C_{22}H_{12}$, the B2PLYP

results are in better agreement with reference data, while the MP2 overstabilizes the singlet state. On the other hand, both B2PLYP and MP2 approaches predict the singlet closed-shell state as more stable for $C_{46}H_{18}$ than the other higher states. If one excludes the singlet closed shell, MP2 and B2PLYP also indicate the quintet as the ground state, even though the B2PLYP difference between triplet and quintet states is very small. It is not of our knowledge the synthesis or simulation of triangulene $C_{33}H_{15}$, but it is possible it has a quartet character in the ground state, as predicted by BLYP and MP2.

As observed before for the singlet–triplet gap (Table 1 and Refs. [26, 51]), the MP2 difficulties in predicting the adequate multiplicity of polyradicaloids is a consequence of applying perturbation theory to poor UHF data reference and, in fact, our UHF calculations indicate high spin contamination also for these systems. The double-hybrid functional, B2PLYP, is less affected by the problems in the UHF reference state. The results obtained using the B3LYP functional adequately predict the correct order of stability for the different multiplicity forms.

4 Conclusions

Density functional theory and electronic structure approaches have been used as an efficient methodology to study the molecules stability and the radical species formation. In this work, electronic and energetic aspects of polycyclic aromatic hydrocarbons (PAHs), including triangulenes,

Fig. 3 Structure of studied triangulene derivatives (first row) and respective passivated form (second row) used as reference for BDE calculations

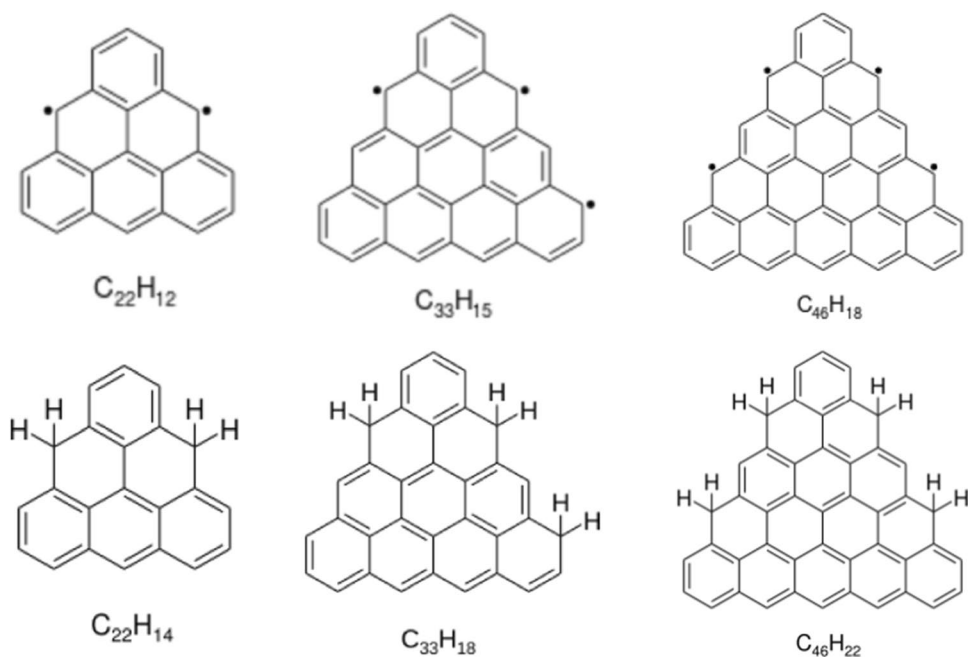
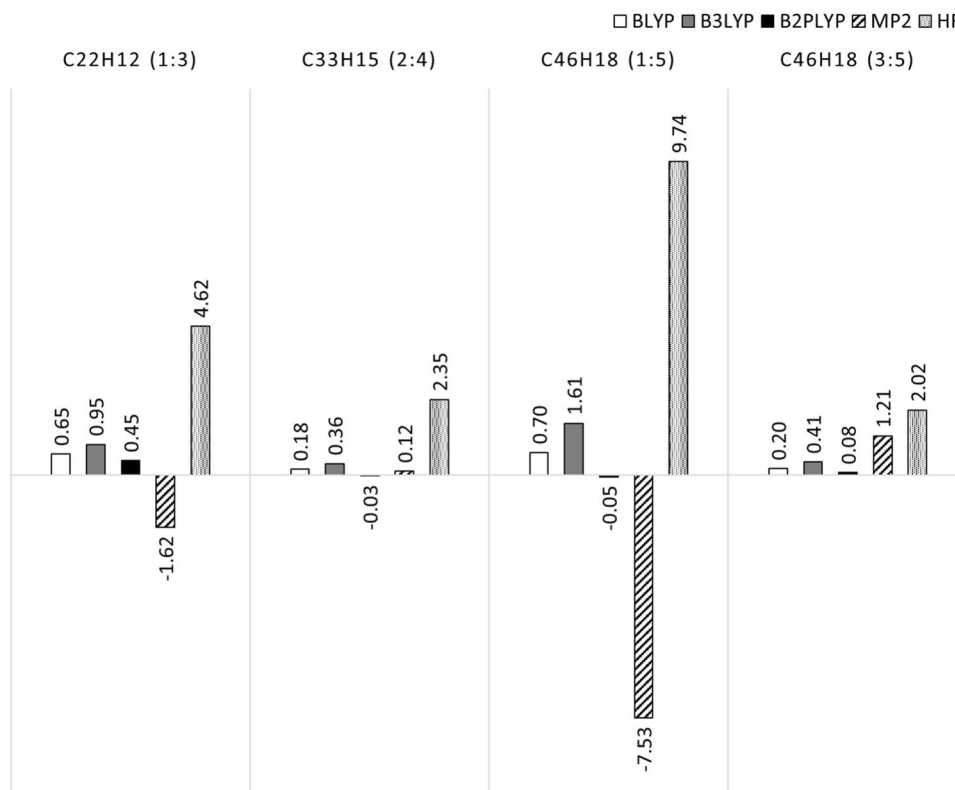


Fig. 4 Relative energies (in eV) regarding the adequate high spin configuration (in parenthesis, “state”: “reference state”) for three triangulene derivatives calculated with BLYP, B3LYP, B2PLYP, MP2, and UHF levels at BLYP geometries



were analyzed with UHF and MP2 theories as well as with BLYP and B2PLYP density functionals.

The singlet–triplet energy gap results of selected PAHs indicate that the description of these excited states is affected by the spin contamination present in the UHF reference state, also used for the MP2 calculations. The overestimation of the MP2 results in contrast to the underestimation of the UHF ones can be rationalized in terms of the slow convergence exhibited by spin contaminated wave-functions. The absence of the UHF reference-state contribution in the BLYP functional composition led to considerable improvement of singlet–triplet energy gaps obtained with this functional. Best results, however, were obtained with the double-hybrid B2PLYP density functional, whose method includes the same correction responsible for the overestimation of the excited-state energies showed by the MP2 calculations. It should be noted that part of the B2PLYP success for this energy gap suggests a compensation between the spin contamination and the MP2 correction, both part of the B2PLYP method.

The bonding dissociation energies (BDE) of the adiabatic homolytic hydrogen withdrawn from different positions of even and odd-numbered carbon atom PAHs were calculated with BLYP and B2PLYP functionals—this analysis included PAHs up to $C_{46}H_{18}$. Although showing the same trend as the preferential site for the hydrogen withdrawn, the difference between BDE obtained with BLYP and B2PLYP for larger

PAHs is considerable. Furthermore, the unrestricted UHF reference state contribution, and its “correction” due to the MP2 part, present into the B2PLYP composition, seems to amplify the BDE differences for different sites considered to have similar chemical characteristics. This result also seems to be related with the spin contamination for B2PLYP.

The BDE values tend to decrease as the PAH structures get larger, although it shows to be less pronounced in the B2PLYP results than in the BLYP ones. This result indicates that spin contamination in the B2PLYP calculation, caused by the UHF and MP2 contributions, destabilizes the generated radical.

As a final remark, the different possible multiplicities that can be achieved by the triangulenes make them interesting PAHs structures from a theoretical point of view. For this class of PAHs, BLYP (and also B3LYP) correctly predicts the most stable multiplicity for the three investigated systems. At the same time, B2PLYP underestimation of energy gaps can be rationalized in terms of the extreme behavior obtained from UHF and MP2 calculations.

Acknowledgements The authors thank the Brazilian agencies Fundação de Apoio à Pesquisa do Estado de São Paulo—FAPESP (17/23416-9), Conselho Nacional de Desenvolvimento Científico e Tecnológico—CNPq (306177/2016-1, 423022/2018-0 and 306585/2019-7) for financial support. This study was financed in part by the Coordenação de Aperfeiçoamento de Pessoal de Nível Superior (CAPES)—Finance Code 001.

Compliance with ethical standards

Conflict of interest All authors declare that they have no conflict of interest.

References

- Reddy SN, Mahapatra S (2015) Theoretical study on molecules of interstellar interest. II. Radical cation of compact polycyclic aromatic hydrocarbons. *J Phys Chem B* 119:11391–11402. <https://doi.org/10.1021/acs.jpcc.5b03614>
- Michoulier E, Ben Amor N, Rapacioli M et al (2018) Theoretical determination of adsorption and ionisation energies of polycyclic aromatic hydrocarbons on water ice. *Phys Chem Chem Phys* 20:11941–11953. <https://doi.org/10.1039/c8cp01175c>
- Michoulier E, Noble JA, Simon A et al (2018) Adsorption of PAHs on interstellar ice viewed by classical molecular dynamics. *Phys Chem Chem Phys* 20:8753–8764. <https://doi.org/10.1039/c8cp00593a>
- Simon A, Spiegelman F (2013) Conformational dynamics and finite-temperature infrared spectra of the water octamer adsorbed on coronene. *Comput Theor Chem* 1021:54–61. <https://doi.org/10.1016/j.comptc.2013.06.023>
- Allison TC, Burgess DR (2015) First-principles prediction of enthalpies of formation for polycyclic aromatic hydrocarbons and derivatives. *J Phys Chem A* 119:11329–11365. <https://doi.org/10.1021/acs.jpca.5b07908>
- Ewa B, Danuta MŚ (2017) Polycyclic aromatic hydrocarbons and PAH-related DNA adducts. *J Appl Genet* 58:321–330. <https://doi.org/10.1007/s13353-016-0380-3>
- Munoz B, Albores A (2011) DNA damage caused by polycyclic aromatic hydrocarbons: mechanisms and markers. *Sel Top DNA Repair*. <https://doi.org/10.5772/22527>
- Lakshman MK, Kole PL, Chaturvedi S et al (2000) Methyl group-induced helicity in 1,4-dimethylbenzo[*c*]phenanthrene and its metabolites: synthesis, physical, and biological properties. *J Am Chem Soc* 122:12629–12636. <https://doi.org/10.1021/ja002072w>
- Shimada T (2006) Xenobiotic-metabolizing enzymes involved in activation and detoxification of carcinogenic polycyclic aromatic hydrocarbons. *Drug Metab Pharmacokinet* 21:257–276. <https://doi.org/10.2133/dmpk.21.257>
- Khatymov RV, Muftakhov MV, Shchukin PV (2017) Negative ions, molecular electron affinity and orbital structure of cata-condensed polycyclic aromatic hydrocarbons. *Rapid Commun Mass Spectrom* 31:1729–1741. <https://doi.org/10.1002/rcm.7945>
- Salvador MA, Sousa CP, Maciel CD et al (2018) Experimental and computational studies of the interactions between carbon nanotubes and ionic liquids used for detection of acetaminophen. *Sensors Actuators B Chem*. <https://doi.org/10.1016/j.snb.2018.09.017>
- Tachikawa H (2017) Hydrogen atom addition to the surface of graphene nanoflakes: a density functional theory study. *Appl Surf Sci* 396:1335–1342. <https://doi.org/10.1016/j.apsusc.2016.11.158>
- Donchev AG (2007) Ab initio study of the effects of orientation and corrugation for H₂ adsorbed on polycyclic aromatic hydrocarbons. *J Chem Phys* 126:1–7. <https://doi.org/10.1063/1.2717174>
- Zhechkov L, Heine T, Seifert G (2011) OPAL: a multiscale multicenter simulation package based on MPI-2 protocol. *Int J Quantum Chem* 111:4020–4029. <https://doi.org/10.1002/qua>
- Wagle D, Kamath G, Baker GA (2013) Elucidating interactions between ionic liquids and polycyclic aromatic hydrocarbons by quantum chemical calculations. *J Phys Chem C* 117:4521–4532. <https://doi.org/10.1021/jp310787t>
- Chakarova-Käck SD, Vojvodica A, Kleis J et al (2010) Binding of polycyclic aromatic hydrocarbons and graphene dimers in density functional theory. *New J Phys* 12:013017. <https://doi.org/10.1088/1367-2630/12/1/013017>
- Das A, Pinheiro M, Machado FBC et al (2018) Tuning the biradicaloid nature of polycyclic aromatic hydrocarbons: the effect of graphitic nitrogen doping in zethrenes. *ChemPhysChem* 19:2492–2499. <https://doi.org/10.1002/cphc.201800650>
- Nieman R, Das A, Aquino AJA et al (2017) Single and double carbon vacancies in pyrene as first models for graphene defects: a survey of the chemical reactivity toward hydrogen. *Chem Phys* 482:346–354. <https://doi.org/10.1016/j.chemphys.2016.08.007>
- Rapacioli M, Spiegelman F, Talbi D et al (2009) Correction for dispersion and Coulombic interactions in molecular clusters with density functional derived methods: application to polycyclic aromatic hydrocarbon clusters. *J Chem Phys* 130:1–10. <https://doi.org/10.1063/1.3152882>
- Silva NJ, Machado FBC, Lischka H, Aquino AJA (2016) π - π stacking between polyaromatic hydrocarbon sheets beyond dispersion interactions. *Phys Chem Chem Phys* 18:22300–22310. <https://doi.org/10.1039/c6cp03749f>
- Parac M, Grimme S (2003) A TDDFT study of the lowest excitation energies of polycyclic aromatic hydrocarbons. *Chem Phys* 292:11–21. [https://doi.org/10.1016/S0301-0104\(03\)00250-7](https://doi.org/10.1016/S0301-0104(03)00250-7)
- Grimme S, Parac M (2003) Substantial errors from time-dependent density functional theory for the calculation of excited states of large *p* systems. *Chem Phys Chem*. <https://doi.org/10.1002/cphc.200390047>
- Buragohain M, Pathak A, Hammonds M, Sarre PJ (2013) Theoretical quantum chemical study of protonated—deuteronated PAHs: interstellar implications. In: AIP conference proceedings, pp 258–264
- Powell J, Heider EC, Campiglia A, Harper JK (2016) Predicting accurate fluorescent spectra for high molecular weight polycyclic aromatic hydrocarbons using density functional theory. *J Mol Spectrosc* 328:37–45. <https://doi.org/10.1016/j.jms.2016.06.015>
- Taylor P, Yadav A, Mishra PC (2013) Molecular physics: an international journal at the interface between chemistry and physics lowest Π - Π^* electronic transitions in linear and two-dimensional polycyclic aromatic hydrocarbons: enhanced electron density edge effect. *Mol Phys* 00:1–8. <https://doi.org/10.1080/00268976.2013.830786>
- Cioslowski J, Liu G, Martinov M et al (1996) Energetics and site specificity of the homolytic C–H bond cleavage in benzenoid hydrocarbons: an ab initio electronic structure study. *J Am Chem Soc* 118:5261–5264. <https://doi.org/10.1021/ja9600439>
- Barckholtz C, Barckholtz TA, Hadad CM (1999) C–H and N–H bond dissociation energies of small aromatic hydrocarbons. *J Am Chem Soc* 121:491–500. <https://doi.org/10.1021/ja982454q>
- Chipem FAS, Dash N, Krishnamoorthy G (2011) Role of nitrogen substitution in phenyl ring on excited state intramolecular proton transfer and rotamerism of 2-(2'-hydroxyphenyl)benzimidazole: a theoretical study. *J Chem Phys*. <https://doi.org/10.1063/1.3562124>
- Pérez-Guardiola A, Ortiz-Cano R, Sandoval-Salinas ME et al (2019) From cyclic nanorings to single-walled carbon nanotubes: disclosing the evolution of their electronic structure with the help of theoretical methods. *Phys Chem Chem Phys* 21:2547–2557. <https://doi.org/10.1039/c8cp06615a>
- Inoue J, Fukui K, Kubo T et al (2001) The first detection of a Clar's hydrocarbon, 2,6,10-tri-tert-butyltriangulene: a ground-state triplet of non-kekulé polynuclear benzenoid hydrocarbon. *J Am Chem Soc* 123:12702–12703
- Haddon RC (1975) Quantum chemical studies in the design of organic metals. III: Odd-alternant hydrocarbons—the phenalenyl

- (ply) system. *Aust J Chem* 28:2343–2351. <https://doi.org/10.1071/CH9752343>
32. Morita Y, Suzuki S, Sato K, Takui T (2011) Synthetic organic spin chemistry for structurally well-defined open-shell graphene fragments. *Nat Chem* 3:197–204. <https://doi.org/10.1038/nchem.985>
33. Sharma V, Som N, Dabhi SD, Jha PK (2018) Tailoring the electronic and magnetic properties of peculiar triplet ground state polybenzoid “triangulene”. *Chem Select* 3:2390–2397. <https://doi.org/10.1002/slct.201703054>
34. May K, Unterreiner BV, Dapprich S, Ahlrichs R (2000) Structures, C–H and C–CH₃ bond energies of hydrogenated polycyclic aromatic hydrocarbons. *Phys Chem Chem Phys* 2:5084–5088. <https://doi.org/10.1039/b005597m>
35. Møller C, Plesset MS (1934) Note on an approximation treatment for many-electron systems. *Phys Rev* 46:618–622. <https://doi.org/10.1103/PhysRev.46.618>
36. Sæbø S, Almlöf J (1989) Avoiding the integral storage bottleneck in LCAO calculations of electron correlation. *Chem Phys Lett* 154:83–89. [https://doi.org/10.1016/0009-2614\(89\)87442-1](https://doi.org/10.1016/0009-2614(89)87442-1)
37. Head-Gordon M, Head-Gordon T (1994) Analytic MP2 frequencies without fifth-order storage. Theory and application to bifurcated hydrogen bonds in the water hexamer. *Chem Phys Lett* 220:122–128. [https://doi.org/10.1016/0009-2614\(94\)00116-2](https://doi.org/10.1016/0009-2614(94)00116-2)
38. Hohenberg P, Kohn W (1964) Inhomogeneous electron gas. *Phys Rev* 136:B864. <https://doi.org/10.1103/PhysRev.136.B864>
39. Kohn W, Sham LJ (1965) Self-consistent equations including exchange and correlation effects. *Phys Rev* 140:A1133. <https://doi.org/10.1103/PhysRev.140.A1133>
40. Parr RG, Weitao Y (1989) Density-functional theory of atoms and molecules. Oxford University Press, Oxford
41. Neese F (2012) The ORCA program system. *Wiley Interdiscip Rev Comput Mol Sci* 2:73–78. <https://doi.org/10.1002/wcms.81>
42. Neese F (2018) Software update: the ORCA program system, version 4.0. *Wiley Interdiscip Rev Comput Mol Sci* 8:4–9. <https://doi.org/10.1002/wcms.1327>
43. Becke AD (1988) Density-functional exchange-energy approximation with correct asymptotic-behavior. *Phys Rev A* 38:3098–3100. <https://doi.org/10.1103/PhysRevA.38.3098>
44. Lee C, Yang W, Parr RG (1988) Development of the Colle–Salvetti correlation-energy formula into a functional of the electron density. *Phys Rev B* 37:785–789. <https://doi.org/10.1103/PhysRevB.37.785>
45. Grimme S, Antony J, Ehrlich S, Krieg H (2010) A consistent and accurate ab initio parametrization of density functional dispersion correction (DFT-D) for the 94 elements H–Pu. *J Chem Phys* 132:154104. <https://doi.org/10.1063/1.3382344>
46. Liu S, Ma Y-Z, Yang Y-F et al (2018) Excited state intramolecular proton transfer mechanism of *o*-hydroxynaphthyl phenanthroimidazole. *Chin Phys B*. <https://doi.org/10.1088/1674-1056/27/2/023103>
47. Mineo H, Fujimura Y (2017) Quantum control of coherent π -electron ring currents in polycyclic aromatic hydrocarbons. *J Chem Phys* doi. <https://doi.org/10.1063/1.5004504>
48. Sure R, Brandenburg JG, Grimme S (2016) Small atomic orbital basis set first-principles quantum chemical methods for large molecular and periodic systems: a critical analysis of error sources. *Chem Open* 5:94–109. <https://doi.org/10.1002/open.201500192>
49. Grimme S, Ehrlich S, Goerigk L (2011) Effect of the damping function in dispersion corrected density functional theory. *J Comput Chem* 32:1456–1465. <https://doi.org/10.1002/jcc.21759>
50. Huzak M, Hajgató B, Deleuze MS (2012) Benchmark theoretical study of the ionization energies, electron affinities and singlet–triplet energy gaps of azulene, phenanthrene, pyrene, chrysene and perylene. *Chem Phys* 406:55–64. <https://doi.org/10.1016/j.chemphys.2012.08.003>
51. Becke AD (1993) Density-functional thermochemistry. III. The role of exact exchange. *J Chem Phys* 98:5648–5652. <https://doi.org/10.1063/1.464913>
52. Vosko SH, Wilk L, Nusair M (1980) Accurate spin-dependent electron liquid correlation energies for local spin density calculations: a critical analysis. *Can J Phys* 58:1200–1211. <https://doi.org/10.1139/p80-159>
53. Stephens PJ, Devlin FJ, Chabalowski CF, Frisch MJ (1994) Ab Initio calculation of vibrational absorption and circular dichroism spectra using density functional force fields. *J Phys Chem* 98:11623–11627. <https://doi.org/10.1021/j100096a001>
54. Gill PMW, Pople JA, Radom L, Nobes RH (1988) Why does unrestricted Møller–Plesset perturbation theory converge so slowly for spin-contaminated wave functions? *J Chem Phys* 89:7307–7314. <https://doi.org/10.1063/1.455312>
55. Perumal S, Minaev B, Ågren H (2012) Spin–spin and spin–orbit interactions in nanographene fragments: a quantum chemistry approach. *J Chem Phys*. <https://doi.org/10.1063/1.3687002>
56. Menon AS, Radom L (2008) Consequences of spin contamination in unrestricted calculations on open-shell species: effect of Hartree–Fock and Møller–Plesset contributions in hybrid and double-hybrid density functional theory approaches. *J Phys Chem A* 112:13225–13230. <https://doi.org/10.1021/jp803064k>
57. Son YW, Cohen ML, Louie SG (2006) Energy gaps in graphene nanoribbons. *Phys Rev Lett* 97:1–4. <https://doi.org/10.1103/PhysRevLett.97.216803>
58. Su J, Telychko M, Hu P et al (2019) Atomically precise bottom-up synthesis of π -extended [5]triangulene. *Sci Adv*. <https://doi.org/10.1126/sciadv.aav7717>
59. Pavliček N, Mistry A, Majzik Z et al (2017) Synthesis and characterization of triangulene. *Nat Nanotechnol* 12:308–311. <https://doi.org/10.1038/nnano.2016.305>

Publisher's Note Springer Nature remains neutral with regard to jurisdictional claims in published maps and institutional affiliations.